Title: Unraveling the role of electron-hole pair spin in exciton dissociation in squaraine-based organic solar cells by magneto-photocurrent measurements

Maciej Klein[a, b]*, *Sayani Majumdar* [c, d], *Paweł Zassowski* [e], *Waldemar Stampor* [a]

[a] Department of Physics of Electronic Phenomena, Faculty of Applied Physics and Mathematics, Gdansk University of Technology, 80-233 Gdansk, Poland

[b] Distributed Energy Department, The Szewalski Institute of Fluid-Flow Machinery, Polish Academy of Sciences, 80-231 Gdansk, Poland

[c] NanoSpin, Department of Applied Physics, Aalto University School of Science, FI-00076 Aalto, Finland

[d] Wihuri Physical Laboratory, Department of Physics and Astronomy, University of Turku, FI-20014 Turku, Finland

[e] Faculty of Chemistry, Silesian University of Technology, 44-100 Gliwice, Poland

Abstract

A high absorption coefficient and a narrow absorption band in squaraine (SQ) dyes have resulted in rapidly growing interest in them as a donor material in photovoltaic devices. The exciton dissociation process in organic systems proceeds *via* a multistep mechanism where the electron-hole pairs (charge transfer states) involved in the current generation process determine the recombination losses and subsequently limit the overall performance of organic solar cells. In this work, these basic electronic processes are investigated by magneto-photocurrent measurements (MPC, the photocurrent change induced by the external magnetic field) of SQ:$PC_{60}BM$ bulk-heterojunction solar cells with varying electron acceptor concentration under magnetic fields up to 9 T and at different temperatures. Under weak external magnetic field, the change in photocurrent is due to electron and hole (e-h) pairs that experience a modulating hyperfine interaction associated with nuclear (mainly proton) magnetic moment, while in strong magnetic fields the photocurrent is affected by the Δg mechanism with spin dephasing due to different Lande factors of electron and hole entities ($\Delta g \approx 10^{-3}$). To consistently interpret the amplitudes and lineshapes of MPC signals at various temperatures, the charge carrier hopping in disordered environment competing with the magnetic dipole spin precession is proposed. The requirements for efficient small-molecular weight organic:fullerene bulk-heterojunction solar cells are briefly discussed.

A. Introduction

Over the last few years, the interest in squaraine (SQ) dyes as a donor material for photovoltaic (PV) applications has grown rapidly[1,2]. It is associated with the unique photophysical properties of these organic compounds: a high absorption coefficient (approximately 10^5 cm^{-1}) and narrow absorption bands only in the visible-near infrared region (from ~550 nm even up to ~1000 nm)[3,4]. Due to relatively simple synthesis routes, various derivatives of SQ dye have been developed and found to be applicable in new generation PV technologies: dye-sensitized solar cells (DSSCs), organic photovoltaic (OPV) devices with both

planar (PHJ) and bulk-heterojunction (BHJ) architectures as well as perovskite solar cells (PSC)[1]. The last decade has observed a sharp rise in the photoconversion efficiency (PCE) of these devices (5.9% and 6.1% for SQ:fullerene in PHJ[5] and BHJ[6] architecture, respectively, 8.3% for SQ/polymer/fullerene tandem solar cells[7] and over 10% for the quaternary organic solar cells[2]) that indicate that SQ:fullerene based OPV cells have a significant potential for future commercial applications. Moreover, the squaraine has been considered as a possible material for spintronic applications[8]. Rather short exciton diffusion length ($L_D \leq 2$ nm[9]) and low charge carrier mobility in SQ thin films, in comparison to those in $PC_{70}BM$ (phenyl-C_{70}-butyric acid methyl ester, $L_D = 20$ to 40 nm[10]), implied promise for use of SQ:fullerene blends with the compositional ratio strongly favoring fullerene (best photoconversion efficiencies, 5.5%, obtained for 1:6 SQ to fullerene weight ratio)[10]. Even though the observed low fill factors (FF) for current-voltage characteristics suggest that the process of exciton dissociation / carrier pair recombination to be field-dependent[11], nevertheless, the authors of ref.[12] argue that in such systems with the poor transport properties (high internal resistance and the short length of exciton diffusion in SQ) low charge collection governs cell performance.

Nowadays, further improvement of organic solar cells performance can be achieved by applying the following strategies: (i) tuning or broadening the absorption band of photoactive materials for better matching with the solar spectrum[1]; (ii) employing new device architectures, especially tandem solar cells[13], maximizing an open circuit voltage (V_{oc}) by appropriate energy levels alignment, namely, a charge transfer level (in donor-acceptor systems) should lie close to a singlet state of a donor (S_1)[14]; (iii) enhancing photocurrent densities by singlet fission based strategies[15,16]; (iv) enabling the suppression of electron-hole recombination by taking into account the interplay between spin, energetics and delocalization of electronic excitations[17]. The primary step of photocurrent generation in organic solar cells is a dissociation of photogenerated excitons by charge transfer across the donor-acceptor interface leading to the formation of bound interfacial charge transfer (CT) states where an electron and a hole are

located on separate molecules, an acceptor and a donor, respectively. Such bound charge pairs can dissociate into free carriers forming a photocurrent or restore the ground state by means of geminate recombination[17,18]. Due to larger separation distance of electron-hole (e-h) pairs, compared to the molecular excitons, relatively weak electrostatic electron exchange interactions result in CT states of singlet ^{1}(CT) and triplet ^{3}(CT) spin character, almost degenerate in energy. Therefore, the role of spin of electronic excitations is essential when considering possible pathways for both photocurrent generation and recombination losses in photovoltaic devices[17–19].

Recently, magnetic field effects (MFEs) technique has been recognized as a powerful tool for studying spin-dependent generation and recombination processes of spin-pair species in organic semiconductor or polymer based solar cells and light emitting diodes[19–26]. In the state-of-the-art polymer donor:PC$_{60}$BM devices, depending on PC$_{60}$BM ([6,6]-Phenyl-C$_{60}$-butyric acid methyl ester) concentration and external magnetic field strength, various MFEs on a photocurrent (called magneto-photocurrent, MPC) have been observed. For a pristine P3HT (poly(3-hexylthiophene)) or its blend with a low PC$_{60}$BM concentration (<1 wt.%) in a low magnetic field (a few militesla) positive component of MPC is related to the hyperfine interaction modulation (HFM) in (e-h) pairs while negative component at higher magnetic field (tens of militesla) reflects exciton-charge reactions (T-q model) occurring in the triplet excitonic states[21]. Similar effects have been reported for blends with a poly(2-methoxy-5-(3,7-dimethyloctyloxy)-1,4-phenylenevinylene) (MDMO-PPV) as a donor[22]. Intermediate concentrations of PC$_{60}$BM (30-60 wt.%) leads to form CT states at the donor-acceptor interface[22,23] whereas for a high PC$_{60}$BM content (over 70%) strong phase separation occurs and only negative MFE at low magnetic field, outlined as a bipolaron (BP) mechanism, is present[22]. In a previous work[21], MPC at high magnetic field (ca. 1 T) and intermediate PC$_{60}$BM content is reported to be related to the CT states without the specification of exact mechanism of magnetic field effects. However, a few other reports[22,23], suggested that MPC is associated

with the dephasing of spin magnetic dipoles due to different values of Lande g factor ($\Delta g \sim 10^{-3}$) for electron and hole entities forming CT states, referred to as the Δg mechanism. In our earlier work[27] we examined MFEs in dye-sensitized solar cells with SQ2 adsorbed on TiO_2 semiconductor where small negative MPC signals already observed under weak external magnetic field were ascribed to the Δg mechanism due to the relatively low g value of Ti^{3+} electron center in semiconductor material.

In the present work, we focus on the exciton dissociation and charge carriers recombination processes in $SQ{:}PC_{60}BM$ organic solar cells based on the studies of the magnetic field effects on photocurrent. We address the role of e-h pair states and CT states in OPV cells with various $PC_{60}BM$ concentration presenting a detailed photocurrent generation mechanism for both single-layer and bulk-heterojunction solar cells. Depending on temperature and active layer content, the different components operating in the ultrasmall (<3 mT), hyperfine (<10 mT), fine (<100 mT) and high (of the order of several tesla) magnetic field range contribute to the overall MPC signal. To the best of our knowledge, we report here for the first time on the magnetic field effects in small-molecular weight organic:fullerene bulk-heterojunction solar cells and unravel the mechanism underlying these effects in a wide range of magnetic field strength.

B. Experimental

Materials. SQ2 and $PC_{60}BM$ were purchased from Solaronix and Lumtec, respectively, and were used as received without any additional purification.

Device Fabrication. $SQ{:}PC_{60}BM$ devices were fabricated on etched ITO coated glass substrates (resistivity = 100 Ω/sq) which were cleaned using sequentially acetone, ethanol and deionized (DI) water 10 min each in ultrasonic bath and then dried under a stream of dry nitrogen followed by ozone treatment for 15 min. Afterwards substrates and materials were transferred into nitrogen-filled glove box ([O_2]<1 ppm, [H_2O]<1 ppm). The SQ2 and $PC_{60}BM$ were separately dissolved in anhydrous chlorobenzene (99.8%, Aldrich) at 60℃ overnight and

were then mixed in order to prepare appropriate SQ2 to $PC_{60}BM$ weight ratios. The solutions were heated at 60°C for 2 h just prior to spin coating. ITO glass substrates were then transferred to the vacuum system connected directly with the glove box and the 8 nm thick MoO_x layer was thermally evaporated at a base pressure of ~10^{-6} Torr. Afterwards SQ, SQ:PCBM (1:0.1%), SQ:PCBM (1:10%), SQ:PCBM (1:6) thin films were spin coated from 10, 10, 11 and 42 mg mL^{-1} solutions at a rate of 1500, 1500, 1500 and 1000 rpm for 90 s giving active layers thickness around 20, 20, 23 and 75 nm (as determined by using a Tencor Alpha Step 500 Profilometer), respectively. The films were then annealed at 110°C for 10 min. The devices were completed by thermally evaporating a cathode, consisting of 8 Å LiF and 60 nm Al, through a shadow mask in a vacuum system with a base pressure of ~10^{-6} Torr.

Photovoltaic Performance. Photocurrent density-photovoltage (J-V) curves were recorded under 100 mW cm^{-2} AM 1.5 G illumination conditions in ambient air on a Keithley 2400 SourceMeter.

Absorption Spectroscopy. Active layers for UV-VIS absorption and thickness measurements were deposited onto microscopic glass slides in the similar manner as for the device preparation. Absorbance spectra were registered by a Lambda 35 UV-VIS spectrophotometer (Perkin-Elmer) applying appropriate background subtraction.

Photoluminescence Spectra. Phosphorescence measurements of SQ2 were performed in a homemade setup consisting of helium cryostat and 0.3 m Czerny-Turner spectrograph (SR303i, Andor) equipped with an ICCD camera (DH740, Andor). Samples were excited with a HeNe laser (632.8 nm center wavelength and 2 mW output power). The photoluminescence signal was collected perpendicularly to the sample surface, using a quartz lens, and focused on the entrance of optical fiber. The appropriate optical filters were used to block the excitation light. To enhance the phosphorescence by the external heavy atom (bromine) effect a saturated solution of SQ2 in 1,2-dibromoethane was cooled down to 25 K. Absorbance and fluorescence spectra of 10^{-5} M SQ2 solution in 1,2-dibromoethane were measured at room temperature using

a Lambda 35 UV-VIS spectrophotometer (Perkin-Elmer) and a LS 55 fluorescence spectrometer (Perkin-Elmer), respectively.

EPR measurements: Measurements of a radical cation of SQ2 were performed using a JEOL JES-FA200, X-band CW-EPR (continuous-wave electron paramagnetic resonance) spectrometer, operating at 100 kHz field modulation, coupled with an Autolab PGSTAT100N potentiostat. Measurements were carried out in a glass cell narrowed at the bottom, to provide proper conditions for recording EPR spectra, equipped with a Pt wire working electrode, an Ag wire pseudoreference electrode (calibrated *vs*. Fc/Fc$^+$) and a Pt coil counter electrode. Electrolysis was carried out at the potential corresponding to the first oxidation potential (see Figure S2). The *g* factor of generated radical cations was determined by comparison with a JEOL internal standard (Mn(II) salt), knowing that its third hyperfine line has a *g* factor of 2.03324.

AFM measurements. Samples for atomic force microscopy (Veeco Dimension 5000) operated in tapping mode were prepared exactly as for absorption spectroscopy.

Magnetic field effect measurements: For MFEs measurements devices were transferred through nitrogen filled container to the Quantum Design Physical Property Measurement System (PPMS) equipped with a superconducting magnet and kept in the vacuum (<1 mTorr). The devices were driven at a constant bias voltage U = 0.1 V using a Keithley 6487 Picoammeter Voltage Source and were illuminated by a L658P050 laser diode (658 nm center wavelength and 50 mW output power, ThorLabs) and a few meter long optical fiber introduced into the PPMS chamber. The incident photon flux of approx. 10^{16} cm^{-2}s^{-1} was achieved.

Energy levels. The singlet HOMO (highest occupied molecular orbital) and LUMO (lowest unoccupied molecular orbital) energy levels of SQ2 molecule were taken from the ref.[28] while its triplet level was estimated from the maximum of the phosphorescence emission (cf. Figure S1). Energy levels of PC$_{60}$BM were taken from the ref.[29]. The upper limit of the CT

states energy level (E_{CT}) was calculated from the following formula

$$E_{CT} \approx \left| E_{LUMO}^{A} \right| - \left| E_{HOMO}^{D} \right| = 1.1 \, eV \; .$$

C. Results and Discussion

In this study, we used single-layer solar cells, with the squaraine active layer (Figure 1a), and bulk-heterojunction solar cells (Figure 1b) with the blends of SQ (acting as an electron donor and hole conducting material) and $PC_{60}BM$ (acting as an electron acceptor), with the various wt.% acceptor to donor ratio. The chemical structures of materials applied are shown in Figure 1c,d while the absorption spectra of spin-coated films of pristine SQ and $PC_{60}BM$, and SQ:$PC_{60}BM$ (1:0.1 wt%), SQ:$PC_{60}BM$ (1:6 wt%) blends are depicted in Figure 1f. Figure 1e displays the photocurrent density-photovoltage curves of OPV with the SQ and SQ:$PC_{60}BM$ (1:6) active layer under standard simulated illumination conditions (100 mW/cm^2, AM 1.5). A great enhancement of photocurrent density (J_{sc}, from 1.1 to 7.3 mA/cm^2) and photoconversion efficiencies (PCE of 0.13% and 1.28% for SQ and SQ:$PC_{60}BM$ (1:6), respectively) are clearly seen, which compares well with SQ2/C60 planar-heterojunction solar cells reported previously for the same type of squaraine molecule[30]. The lower value of V_{oc} for single-layer than bulk-heterojunction solar cells is likely induced by the low shunt resistance of thin SQ film subject to possible internal short-circuits. Note that the present OPV devices were not optimized for the best performance being fabricated without any carrier blocking buffer layers (that significantly enhance the cell performance up to 6%[6,10]) to track and unravel MFEs on as simple as possible photovoltaic systems.

In the following sections, MFE technique is applied to examine exciton dissociation and charge carriers recombination processes in systems under investigation. The MPC(B) response is given by

$$MPC(B) = \frac{j(B) - j(0)}{j(0)}, \tag{1}$$

8

where the respective terms represent photocurrent with and without magnetic field ($j(B)$ and $j(0)$, respectively). For identifying the spin-mixing mechanism involved in the origin of MPC signals the data points have been fitted with a single-Lorentzian or a double-Lorentzian function having the form of

$$MPC = A_{LFE}B^2/(B^2 + B_{LFE}^2)$$

(2)

and

$$MPC = A_{LFE}B^2/(B^2 + B_{LFE}^2) + A_{HFE}B^2/(B^2 + B_{HFE}^2),$$

(3)

respectively. In the relevant components of the formula (1) and (2) representing the low-field (LFE) and high-field (HFE) effects, A_{LFE} and A_{HFE} parameters denote the MPC signal magnitudes for $B \to \infty$ whereas B_{LFE} and B_{HFE} determine the half width ($B_{1/2}$) at half signal maximum (HWHM)[27,31]. Finally, we discuss possible routes of photophysical processes responsible for observed MFEs.
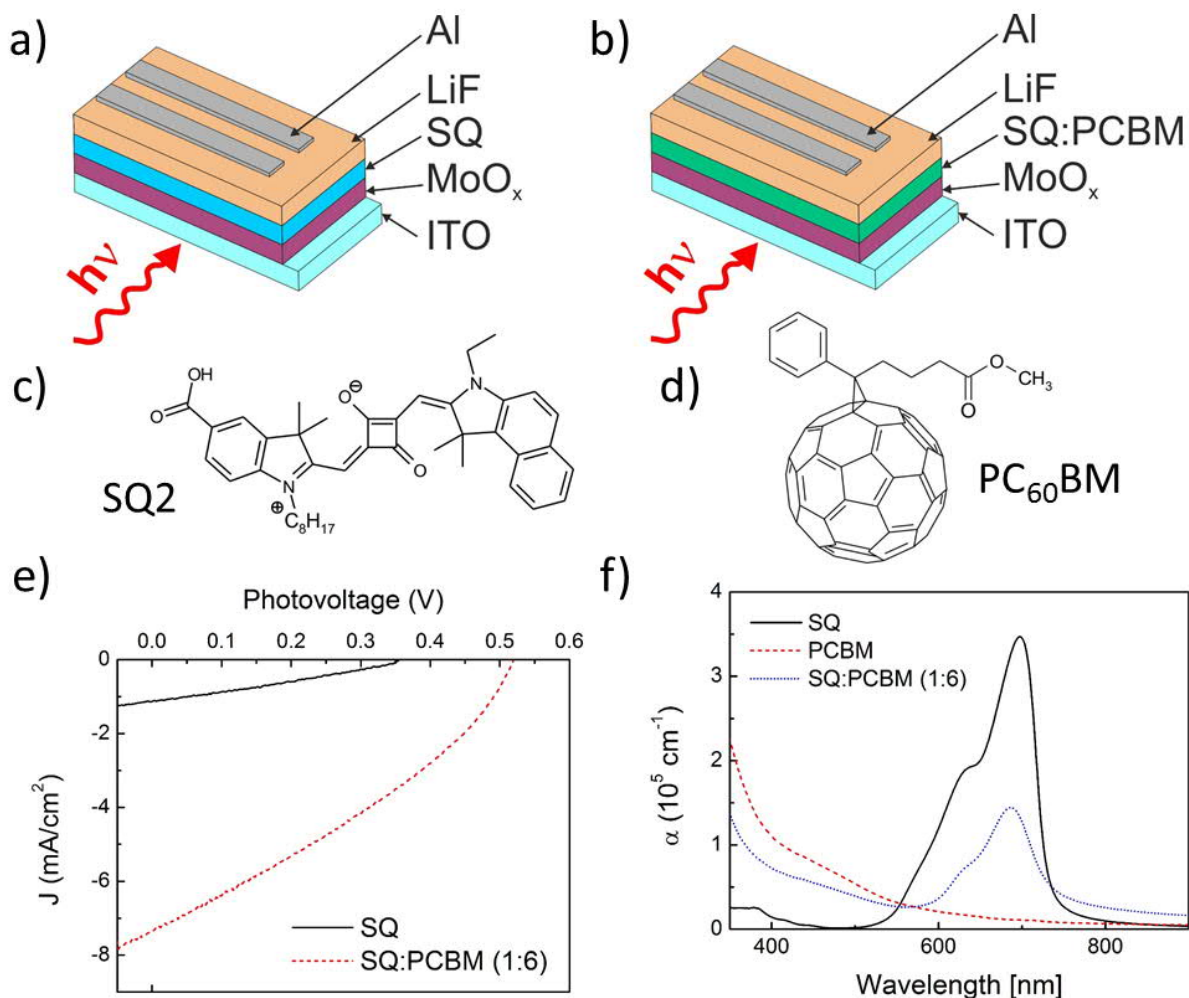
Figure 1. The structure of a single-layer (a) and a bulk-heterojunction (b) solar cell; the chemical structures of squaraine dye SQ2 (c) and fullerene derivative $PC_{60}BM$ (d); the photocurrent density-photovoltage curves for solar cells: with a SQ (solid line) and SQ:$PC_{60}BM$ 1:6 weight ratio (dashed line) active layer (e); the absorption spectra of SQ (solid line), $PC_{60}BM$ (dashed line) and blend (dotted line) of both materials with SQ to $PC_{60}BM$ 1:6 weight ratio (f)

MFEs in squaraine single-layer solar cells

The magnetic field effect on photocurrent (the MPC signal) recorded as a function of the external magnetic field strength for two different temperatures in a sandwiched configuration, ITO/MoO$_x$/SQ/LiF/Al, for the low-field and the ultrasmall-field regime have been depicted in Figure 2a and Figure 2b, respectively. At room temperature (290 K), the MPC signal saturates

on a characteristic for hyperfine interactions magnetic field scale (B_{LFE} = 4 mT) while at lower temperature (200 K), besides the low-field component (B_{LFE} = 3 mT), also the medium-field component (B_{MFE} = 30 mT) appears (Figure 2a). Thus, at 290 K, according to electron-hole pair (EHP) model[20,32–35], the external magnetic field suppresses the spin-mixing occurring at a hyperfine-field scale and consequently increases singlet, ^{1}(e-h), to triplet, ^{3}(e-h), electron-hole pairs (polaron pairs) population ratio in a squaraine molecule. At reduced temperature, gradually increased population of triplets begins to play more important role due to deactivation of radiationless decay pathways. Therefore, at 200 K, besides the low-field effect (induced by HFM), another mechanism likely associated to the fine structure modulation (FSM) becomes active at higher magnetic field. When the external magnetic field competes with the internal (fine) magnetic field of electronic spin origin, it starts to modulate the molecular triplet (T) zero-field splitting (ZFS) and thus changes the free carrier mobility. This triplet-charge interaction (T-q mechanism), proposed as origin of magnetoresistance in organic semiconductors (organic magnetoresistance, OMAR) by Cox *et al.*[36] and called trion model, has been discussed in our previous work[31] (see also ref.[37]). Accordingly, the doublet and quartet trions are formed by interaction between spin-1/2 free charge carriers and spin-1 triplet molecular excitons, T, (presumably trapped in defect sites of an organic solid) populated in the SQ layer. Essential condition for the functionality of this model is that the trions operate as free-carrier-capturing centers hindering the carrier mobility. As a consequence, the overall process may be interpreted as a scattering of free carriers on triplet states. Since the recombination process of doublet trions is spin-allowed with the recombination of the quartet trions remaining spin-forbidden, the lifetime of the doublet trions is much shorter than that of quartet ones. Therefore, the quartet trions are more efficient in capturing free carriers and, hence, in reducing the photocurrent. Importantly, in the FSM-scale magnetic field of the several-tens-of-mT, the population of the quartet trions is reduced whereas the population of the doublet ones increases. This leads to the lower contribution of the quartet trions and, simultaneously, higher

contribution of the doubling trions to the overall scattering process. One, therefore, should observe the increase in photoconductivity of an organic solid due to rising mobility of charge carriers which is the case from Figure 2a. Another issue which we would like to explain is the amplitude enhancement of low-field component due to temperature reduction. Nevertheless, first we shall note that the external magnetic field can change the intersystem crossing rate in electron-hole pair intermolecular states (ISC_{eh}) but has little influence on this rate in intramolecular excitonic states (ISC_{ST}) with larger singlet-triplet splitting energy[38]. Therefore, on the one hand an increase in the amplitude of the MPC signal originated from carrier scattering on molecular triplets can be induced by the low magnetic field associated with the HFM mechanism, namely, the external magnetic field operating on hyperfine scale reduces population of T excitons formed from ^{3}(e-h) states thereby enhances the mobility of free charge carriers. However, on the other hand another explanation of the amplitude change, which is in a good agreement with other results presented later in the text, is also possible. If we assume that the charge carrier hopping frequency (ω_{hop}) is in the order of hyperfine precession frequency (ω_{hf}), i.e. $\omega_{hf} / \omega_{hop} \approx 1$ (intermediate-hopping regime), then reducing the temperature, and thereby also reducing the hopping frequency, will be reflected in the MPC signal amplitude increase and a decrease in its linewidth[39]. Indeed, a slight change in the width of a low-field Lorentz component with temperature reduction, from $B_{LFE} = 4$ mT to $B_{LFE} = 3$ mT, has been observed. Nevertheless, it may be also associated with the reduction of the broadly distributed decay times of (e-h) pairs in such disordered materials as those used in OPV cells[23].

Let us now take a closer look at the 0-3 mT magnetic field strength range (Figure 2b). The ultrasmall magnetic field effect (USMFE), with the opposite sign than the low-field effect can be easily recognized. This intrinsic effect in OMAR according to semiclassical approach proposed by Koopmans and co-workers[39] originates from the competition between spin mixing and exciton formation for intermediate-hopping rates. On the other hand, to investigate the

observed MPC line shapes, Vardeny and co-workers[40] applied fully quantum-mechanical approach in which the polaron pair spin Hamiltonian includes the hyperfine interaction between each of the polaron pair constituents and one or more strongly coupled neighboring nuclei. Therefore, existing singlet-triplet (S-T) level-crossing (LC) of (e-h) pair states gives rise to excess spin intermixing between hyperfine-split spin sublevels. The external magnetic field (of ultrasmall magnitude) can change the S-T intermixing rate provided by the hyperfine interaction and this way perturbs the overall relative steady state populations of the spin sublevels. Although the authors found that the amplitude of USMFE increases with increasing temperature with the linewidth remaining unaffected. The quantitative description of temperature dependencies, however, is lacking in that study. According to our findings, the observed ultrasmall effect is rather determined by the carrier hopping process, which is in a good agreement with Koopmans group modeling results[39]. With increasing temperature, the hopping frequency (ω_{hop}) increases, as a result decrease in MPC magnitude and an increase in linewidth are observed.

The MPC signal, measured at 290 K and 20 mT magnetic field strength as a function of forward (negative) and reverse (positive) bias voltage is depicted in Figure 2c. At a bias voltage below (above) V_{oc}, magnetic field effect is positive (negative) and shows a weak dependence on the applied voltages while at voltages close to V_{oc}, large values of MFE and a change of sign occurs. Similar MFE on photocurrent in P3HT:PCBM bulk-heterojunction solar cells has been reported by Shakya et al.[41] and Lei et al.[42] A great enhancement in magnitude of MPC signals at bias voltages around V_{oc} appears due to vanishing j(0) (in formula (1)) as the bias voltage approaches V_{oc}. Moreover, we shall note that no mutual exciton–exciton interactions occur in the SQ layer as the photocurrents are proportional to light intensities used in our measurements and therefore the MPC signals do not depend on incident photon flux (see Figure 2d).
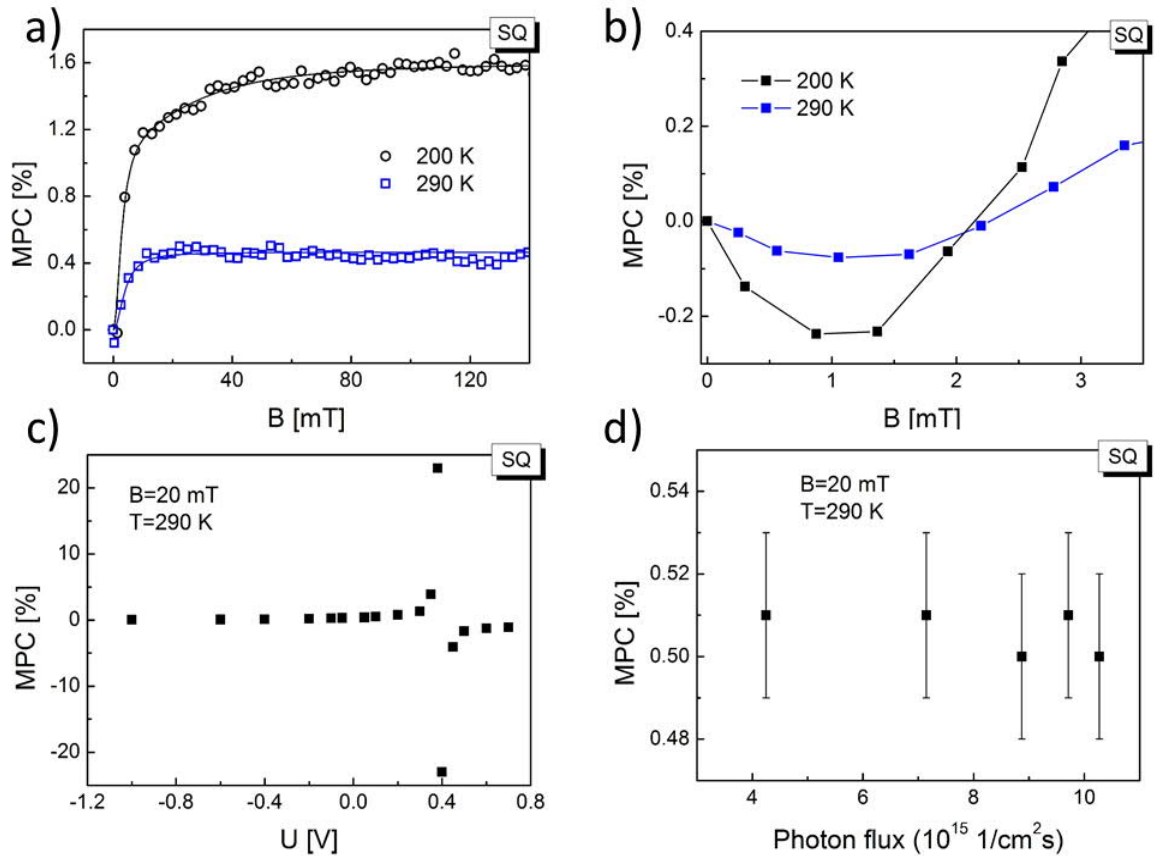
Figure 2. The magnetic field effect on photocurrent for single-layer solar cells. The MPC signal as a function of magnetic field strength for two different temperatures: 200 K (circles) and 290 K (squares) in the low (0-140 mT) and ultrasmall (0-3 mT) field range are displayed in parts (a) and (b), respectively. The MPC signal *versus*: forward (negative) and reverse (positive) bias voltage (c), and photon flux (d) at 20 mT-magnetic field and 290 K temperature are also shown. The solid lines in part (a) represent the best fit according to the single- and double-Lorentzian functions for 290 and 200 K, respectively. The solid line in part (b) is a guide to the eye

MFEs in squaraine:fullerene bulk-heterojunction solar cells

Dependence of MFEs as a function of fullerene concentration in SQ:PC$_{60}$BM bulk-heterojunction solar cells has been investigated (Figure 3a). It can be seen that even a small amount of PC$_{60}$BM (0.1 wt.%) results in a decrease of a positive low-field component

(B_{LFE} = 4 mT) which indicates that $PC_{60}BM$ effectively quenches excitons in SQ layer. Further, the increase in fullerene concentration (up to 10 wt.%) leads to formation of CT states (where the electron resides on the $PC_{60}BM$ and the hole occupies the SQ molecule) which are lower in energy then (e-h) pair states as well as singlet and triplet molecular states of both SQ and $PC_{60}BM$ (cf. Figure 5). The MPC signal with only low-field component (B_{LFE} = 4 mT), similar to the pristine SQ devices, can be easily explained by the EHP model. The sign change (from positive to negative), however, indicates that dissociation of the electronic excited states proceeds this time *via* the CT states and consequently the magnetic field dependent intersystem crossing in CT states (ISC_{CT}) plays a crucial role. Further doping the SQ with $PC_{60}BM$ (up to 1:6 organic to fullerene wt. ratio) reduces the magnitude of the low-field (B_{LFE} = 8 mT) negative MPC signal. In polymer:fullerene blends with such a high $PC_{60}BM$ concentration, phase separation usually occurs[22,29]; then the corresponding MPC signal may be ascribed to the bipolaron (BP) model[43] wherein HFM in charge carrier pairs with the same signs (e-e or h-h) occurs. The atomic force microscopy (AFM) analysis of $SQ:PC_{60}BM$ blends indicates that fullerene is still homogeneously distributed throughout the squaraine (see Figure S5f in the Supplementary Material). Therefore, the bipolaron model operating in $PC_{60}BM$ domains may be safely neglected. We believe that here hyperfine spin mixing in CT states (EHP model) is still valid while the decrease of the MPC signal, in comparison to the small $PC_{60}BM$ concentration system (10 wt.% $PC_{60}BM$), is associated with reduction in the amount of active $SQ:PC_{60}BM$ interfaces.

The half-width of magnetic field dependence of MPC signal for samples with high $PC_{60}BM$ content should be essentially lower than in pristine SQ due to the vanishing nuclear magnetic moment of ^{12}C as reported for MDMO-PPV:$PC_{60}BM$ system[22]. Although in our investigation a completely opposite behavior (B_{LFE} = 8 mT and B_{LFE} = 4 mT for blends and pristine SQ, respectively) is observed, nevertheless this finding corroborates our previous assignment of carrier hopping frequency to intermediate regime ($\omega_{hop} \approx \omega_{hf}$). Then, the MPC linewidths are

determined not only by the hyperfine field but also by the lifetimes of diffusively moving e-h pairs in a solid environment exhibiting various types of structural disorder[39].

In the following section, we focus on the SQ:PC$_{60}$BM 1:6 wt. ratio system for which the highest photoconversion efficiency has been reported so far. The negative MPC signal recorded at various temperatures (200, 250 and 290 K) saturates at low-field scale and remains constant until about 200 mT. Above 200 mT, the absolute MPC value starts to decrease and at about 600 mT, the signal changes the sign (Figure 3b and Figure 4a). With increase in magnetic field strength the positive high-field component, rather weakly affected by the temperature, increases and does not saturate up to 9 T. Moreover, reducing the temperature the amplitude of low-field negative component increases and its linewidth decreases (B$_{LFE}$ = 8 mT and B$_{LFE}$ = 4 mT for 290 and 200 K, respectively) which once more emphasizes substantial influence of thermally activated hopping frequency on the MPC signals (Figure 3b).

In order to clarify the origin of the high-field component we have measured the Lande g factor for a hole (g_h) localized onto SQ2 molecule by the electron paramagnetic resonance, EPR, (Figure S3) and compared it with the g factor value taken from the literature for an electron (g_e) placed on a PC$_{60}$BM cage[44]. It was found that $g_h = 2.0042$ and $g_e = 1.9996$, leading to $\Delta g = 0.0046$. Presence of the only positive MPC signal in high magnetic field range and a difference in Lande factors of the order of 10^{-3} indicate that the so called Δg mechanism may be potentially involved as similarly considered for MPC effect in P3HT:PC$_{60}$BM photovoltaic cells ($\Delta g = 0.002$)[23]. In the EHP model a difference in precession frequency ($\Delta \omega_p$) can be induced not only by a difference in local (of hyperfine origin) magnetic fields (ΔB) experienced by electron and hole entities forming (e-h) pairs ($\Delta \omega_p = g \mu_B \Delta B / \hbar$) but also by a difference in g factors ($\Delta \omega_p = \Delta g \mu_B B / \hbar$), where μ_B is the Bohr magneton, B is the applied field strength and $\hbar$ is the reduced Planck constant. Therefore, in the Δg mechanism the applied magnetic field enhances the intersystem crossing (ISC$_{CT}$) between singlet and $m = 0$ triplet CT states , hence

the corresponding MPC signal have an opposite sign than the LFE induced by HFM[39]. The characteristic lack of pronounced temperature dependence of the high-field component amplitude is a natural consequence of the spin precession - carrier hopping frequency interrelation when the external magnetic field of the order of several tesla enhances significantly the spin precession frequency, ω_p. Therefore, under this regime the precession frequency is definitely greater than the charge carrier hopping frequency ($\omega_p >> \omega_{hop}$); hence a temperature induced change in the hopping rate has no noticeable effect on the MPC signal (Figure 4a). This outcome is significantly different from the results reported for the P3HT:PC$_{60}$BM devices where the signals are strongly temperature dependent[23,45]. To better rationalize the role of CT states in dissociation/recombination decay process, the MPC data at various temperatures were fitted by the Lorentzian functions by means of formulas (1) and (2). The reasonably good fits in the high magnetic field range was obtained using the double-Lorentzian function. According to the formula

$$\tau = \frac{\hbar}{2\mu_B \Delta g B_{1/2}} \tag{4}$$

the CT states relaxation times for 290 K are estimated as 0.82 ns 0.06 ns. Nevertheless, the more appropriate approach should take into account a distribution of relaxation times. It was shown that for a non-exponential (dispersive) relaxation processes the Lorentzian factor, $\text{Re}[1/(1+i\omega_p\tau)]$, may be replaced by the Cole-Cole function, $\text{Re}[1/(1+i\omega_p\tau)^{\alpha}]$, where Re denotes the real part, τ represents an average relaxation time and $\alpha \leq 1$ is the dispersive parameter[23,46]. This can be equivalently interpreted in terms of Kohlrausch-Williams-Watts (KWW) function, the so-called stretched exponential decay, $\exp(-t/\tau)^{\beta}$ with the dispersive β parameter approximately equal to the α parameter from Cole-Cole formula (according to ref.[47] $\alpha \approx \beta^{1.23}$). The respective fit depicted in the Figure 4b gives the $\alpha \approx 0.5$ for temperatures 200-290 K which indicates at a 3D random distribution of CT states decay times[11]. The rather weak

dependence of MPC signals with temperature increase results from a gradual decrease in relaxation time (from $\tau = 1.88$ ns for 200 K to $\tau = 0.57$ ns for 290 K) due to enhancement of all non-radiative decay pathways of CT states including dissociation and geminate recombination processes.

At high magnetic field, besides the Δg mechanism, the thermal spin polarization associated with magnetic field dependence of formation probabilities of singlet and triplet states populated according to the Boltzmann statistics may be also effective. Therefore the spin statistics of the CT states can be substantially controlled by spin-polarizing carriers using high magnetic fields and low temperatures, where the Zeeman energy is comparable with the thermal energy[48]. Therefore, we can calculate the relevant polarizing parameter $b = g\mu_B B / k_B T$ (where k_B is the Boltzmann constant) which gives the maximum spin polarization contribution to the MPC signal as high as $b^2/4 \approx 0.09\%$ (for $g = 2$, B = 9 T and T = 200 K). Hence, comparing this value to the experimentally obtained $MPC\ (B = 9T) \approx 2.2\%$ we can safely neglect spin polarization effects in our considerations. However, this mechanism might be of importance at cryogenic temperatures[45,48].

The MPC signals, just like in the case of single-layer solar cells, do not depend on incident photon flux and again significantly increase and change the sign at the bias voltage around V_{oc} (Figure 3d and Figure 3c, respectively). Moreover, the photocurrent intensity is a linear function of photon flux (Figure 3e).
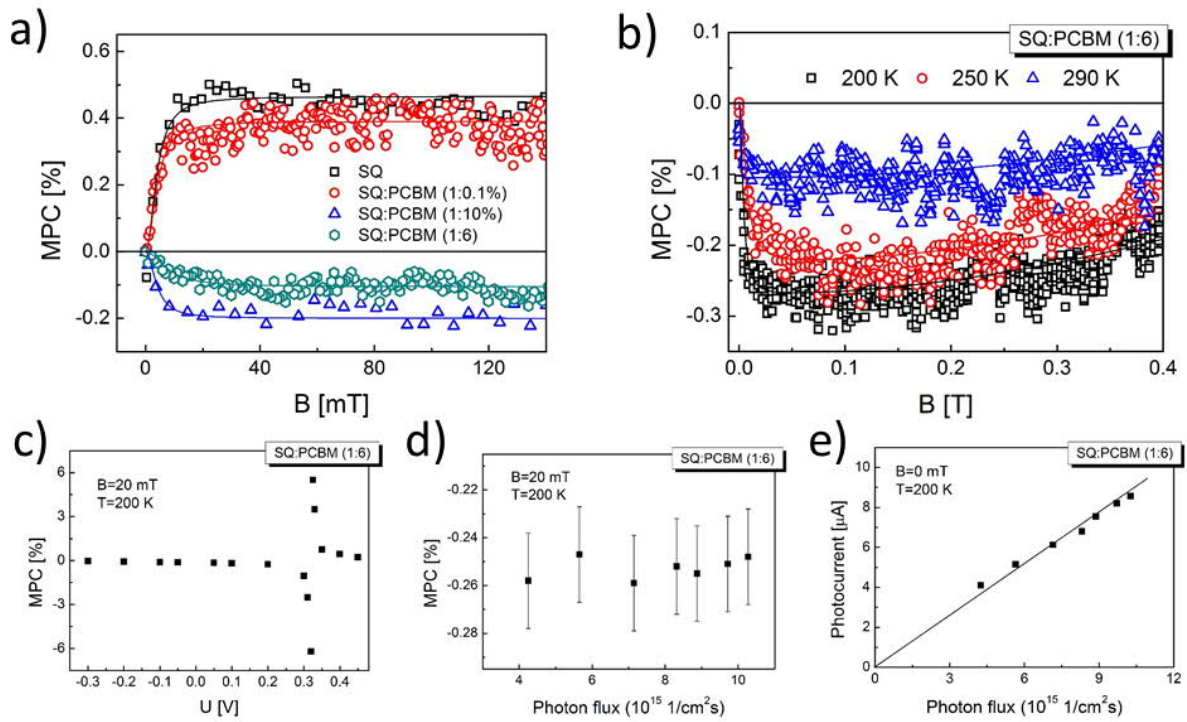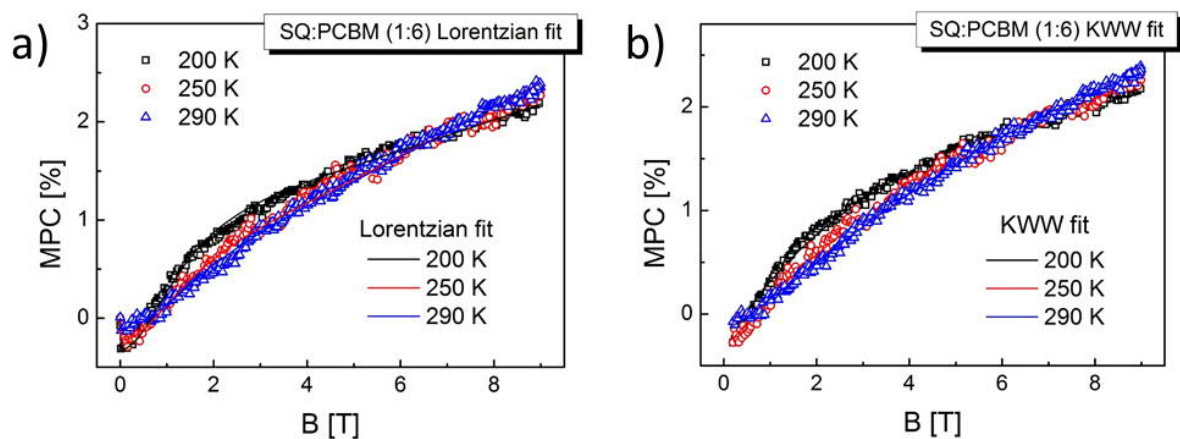
Figure 3. The magnetic field effect on photocurrent for bulk-heterojunction solar cells. The MPC signal as a function of magnetic field strength for various SQ to $PC_{60}BM$ weight ratios at 290 K (a); the MPC signal for a SQ:$PC_{60}BM$ 1:6 wt.% in the medium (0-400 mT) field range for various temperatures (b) are depicted. The MPC signal for a SQ:$PC_{60}BM$ 1:6 wt.% *versus*: forward (negative) and reverse (positive) bias voltage (c), and photon flux (d) at 20 mT-magnetic field and 200 K temperature are also shown. The solid lines in part (a) and (b) represent fit according to the single- and double-Lorentzian functions. In part (e) the light intensity dependence of photocurrent is displayed - the solid line represents a linear fit

Figure 4. The magnetic field effect on photocurrent for bulk-heterojunction solar cells The MPC signals as a function of magnetic field strength for various temperatures are displayed. In part (a) the low-field negative component is approximated using a single-Lorentzian function and the high-field positive component - using a double-Lorentzian function (solid lines). For comparison, in part (b) the best fit of the high-field component applying dispersive relaxation model is shown

The mechanism of magnetic field effects

We consider the following mechanism for explaining the observed magnetic field effects on photocurrent in investigated squaraine:fullerene systems. According to the scheme based on the commonly applied EHP model, the current generation under SQ photoexcitation in single-layer solar cells (Figure 5a) proceeds through intermediate state of e-h pairs. The initially formed ^{1}(e-h) pairs are quasi-degenerated in energy with ^{3}(e-h) pairs due to relatively weak electrostatic exchange interactions at larger distance between electron and hole entities compared to that within molecular (Frenkel type) exciton states. It has been established that singlet/triplet states of e-h pairs (or polaron pairs) can be mixed with each other by hyperfine interactions. When the external magnetic field greater than the hyperfine coupling strength is applied, the Zeeman splitting of triplet states removes the degeneracy between m = ±1 triplet and singlet states, and thus suppresses ^{1}(e-h) → ^{3}(e-h) intersystem crossing increasing population of ^{1}(e-h) pairs. In single component organic solids the dissociation rates (k_{-1}; k_{-3}) differ due to the fact that the singlet pair state has a stronger ionic character than triplets and therefore singlet pair states are more strongly coupled with the ionic reaction products of separated holes and electrons[49], and consequently, to explain MFEs consistently, the $k_{-1} > k_{-3}$ relation is usually assumed[20,35]. In addition, the lower-energy molecular triplet exciton states (operating here as the 'triplet drain'[19]) open efficient recombination pathway for ^{3}CT states, and this way limit the

photocurrent. Further, for MFEs the Lorentzian shape with $B_{1/2}$ width of hyperfine scale is adequate here (cf. Figure 2a) as shown by the quantum mechanical calculations based on Hamiltonian containing the electronic Zeeman interaction with external magnetic field and the hyperfine interaction between a single electronic and nuclear dipole[50].

On the other hand, in bulk-heterojunction solar cells, excited SQ singlet molecular excitons are effectively quenched into ^{1}CT states. Intersystem crossing between singlet and triplet CT states results in forming long-lived ^{3}CT states which are spin-protected from recombination to the ground state due to energetically inaccessible higher lying triplet molecular excitonic states of both squaraine and fullerene molecules (Figure 5b). Contrary to the single component, in electron donor-electron acceptor systems with such energy levels alignment the ^{3}CT dissociation channel in photocurrent generation process is decisive, as recently reported for similar photovoltaic systems[41]. Accordingly, the long-lived triplet CT states exhibit reduced geminate recombination rate and thus enhanced dissociation ability into free charge carriers in P3HT:PCBM devices. Moreover, the comprehensive investigation on the m-MTDATA:3TPYMB system including the direct measurements of CT states fluorescence and photocurrent generation under magnetic field at various pressures also indicates at more efficient triplet channels[19]. A similar outcome has been obtained for polymer (P3HT or MDMO-PPV):fullerene blends at cryogenic temperatures where MFEs of spin polarization origin were investigated[51].
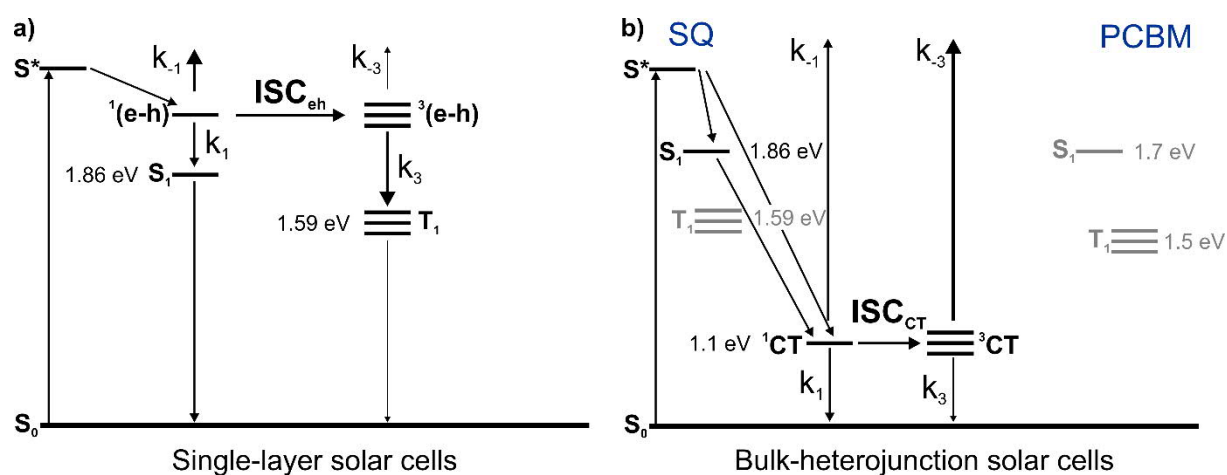

Figure a) Single-layer solar cells; b) Bulk-heterojunction solar cells

Figure 5. Energy diagram of the relevant excited states involved in the photocurrent generation (k_{-1} and k_{-3} reaction rate constants) and charge carrier recombination (k_1 and k_3 reaction rate constants) processes for single-layer (a) and bulk-heterojunction (b) solar cells

D. Conclusions

In summary, a wide range of magnetic field and temperature dependent study of photocurrent in the SQ based solar cells revealed that depending on electron acceptor content, the photocurrent generation is limited by dissociation/recombination of e-h pairs or CT states. Under weak external magnetic field, the HFM mechanism, where an asymmetry in local (of hyperfine origin) magnetic fields experienced by electron and hole forming (e-h) pairs induces spin dephasing of the magnetic dipoles. On the other hand, in strong magnetic field the photocurrent is affected by the Δg mechanism with spin dephasing ascribed to different Lande factors of electron and hole entities. The temperature dependence of the MPC signal indicates that charge carrier hopping in disordered environment plays the essential role in a consistent analysis of MFEs in SQ:PCBM systems. The best performance parameters of solar cells are achieved in systems without molecular 'triplet drains' where dissociation of spin-protected triplet CT states is more favorable. The findings of the present paper enable novel methods to engineer photovoltaic devices utilizing squaraine derivatives, in particular, to determine the alignment of energy levels involved in photocurrent generation process.

AUTHOR INFORMATION

Corresponding Author

*(M. K.) E-mail: mklein@mif.pg.gda.pl

Author Contributions

M.K. prepared samples and performed all experimental measurements (except EPR) and analysis. S. M. supervised samples preparation and magnetic measurements. P. Z. carried out EPR measurements. M.K. and W.S. wrote the manuscript. M. K., S. M. and W. S. discussed the results. All authors have given approval to the final version of the manuscript.

References

1 G. Chen, H. Sasabe, T. Igarashi, Z. Hong and J. Kido, J. Mater. Chem. A, 2015, 3, 14517–14534.

2 T. Goh, J. S. Huang, K. G. Yager, M. Y. Sfeir, C. Y. Nam, X. Tong, L. M. Guard, P. R. Melvin, F. Antonio,

B. G. Bartolome, M. L. Lee, N. Hazari and A. D. Taylor, Adv. Energy Mater., 2016, 6, 1600660.

3 K. Law, J. Phys. Chem., 1987, 91, 5184–5193.

4 F. Silvestri, M. D. Irwin, L. Beverina, A. Facchetti, G. A. Pagani and T. J. Marks, J. Am. Chem. Soc., 2008, 130, 17640–17641.

5 X. Xiao, G. Wei, S. Wang, J. D. Zimmerman, C. K. Renshaw, M. E. Thompson and S. R. Forrest, Adv. Mater., 2012, 24, 1956–1960.

6 G. Chen, H. Sasabe, Z. Wang, X. F. Wang, Z. Hong, Y. Yang and J. Kido, Adv. Mater., 2012, 24, 2768–2773.

7 J. D. Zimmerman, B. E. Lassiter, X. Xiao, K. Sun, A. Dolocan, R. Gearba, D. A. Vanden Bout, K. J. Stevenson, P. Wickramasinghe, M. E. Thompson and S. R. Forrest, ACS Nano, 2013, 7, 9268–9275.

8 Y. Zheng and F. Wudl, J. Mater. Chem. A, 2014, 2, 48–57.

9 G. Wei, R. R. Lunt, K. Sun, S. Wang, M. E. Thompson and S. R. Forrest, Nano Lett., 2010, 10, 3555–3559.

10 G. Wei, S. Wang, K. Sun, M. E. Thompson and S. R. Forrest, Adv. Energy Mater., 2011, 1, 184–187.

11 A. Ko¨hler and H. Ba¨ssler, Electronic Processes in Organic Semiconductors, Wiley-VCH Verlag GmbH & Co. KGaA, Weinheim, Germany, 2015.

12 G. D. Wei, S. Y. Wang, K. Renshaw, M. E. Thompson and S. R. Forrest, ACS Nano, 2010, 4, 1927–1934.

13 A. R. bin Mohd Yusoff, S. J. Lee, H. P. Kim, F. K. Shneider, W. J. da Silva and J. Jang, Adv. Funct. Mater., 2014, 24, 2240–2247.

14 K. Vandewal, K. Tvingstedt, A. Gadisa, O. Inganäs and J. V. Manca, Nat. Mater., 2009, 8, 904–909.

15 S. R. Yost, J. Lee, M. W. B. Wilson, T. Wu, D. P. McMahon, R. R. Parkhurst, N. J. Thompson, D. N. Congreve, A. Rao, K. Johnson, M. Y. Sfeir, M. G. Bawendi, T. M. Swager, R. H. Friend, M. A. Baldo and T. Van Voorhis, Nat. Chem., 2014, 6, 492–497.

16 D. N. Congreve, J. Lee, N. J. Thompson, E. Hontz, S. R. Yost, P. D. Reusswig, M. E. Bahlke, S. Reineke, T. Van Voorhis and M. A. Baldo, Science, 2013, 340, 334–337.

17 A. Rao, P. C. Y. Chow, S. Gélinas, C. W. Schlenker, C.-Z. Li, H.-L. Yip, A. K.-Y. Jen, D. S. Ginger and R. H. Friend, Nature, 2013, 500, 435–439.

18 S. D. Dimitrov, S. Wheeler, D. Niedzialek, B. C. Schroeder, H. Utzat, J. M. Frost, J. Yao, A. Gillett, P. S. Tuladhar, I. McCulloch, J. Nelson and J. R. Durrant, Nat. Commun., 2015, 6, 6501.

19 W. Chang, D. N. Congreve, E. Hontz, M. E. Bahlke, D. P. McMahon, S. Reineke, T. C. Wu, V. Bulović, T. Van Voorhis and M. A. Baldo, Nat. Commun., 2015, 6, 6415.

20 B. Hu and Y. Wu, Nat. Mater., 2007, 6, 985–991.

21 Z. Xu and B. Hu, Adv. Funct. Mater., 2008, 18, 2611–2617.

22 P. Janssen, M. Cox, S. H. W. Wouters, M. Kemerink, M. M. Wienk and B. Koopmans, Nat. Commun., 2013, 4, 2286.

23 A. H. Devir-Wolfman, B. Khachatryan, B. R. Gautam, L. Tzabary, A. Keren, N. Tessler, Z. V. Vardeny and E. Ehrenfreund, Nat. Commun., 2014, 5, 4529.

24 D. Sun, E. Ehrenfreund and Z. Valy Vardeny, Chem. Commun., 2014, 50, 1781–1793.

25 C. Zhang, D. Sun, C.-X. Sheng, Y. X. Zhai, K. Mielczarek, A. Zakhidov and Z. V. Vardeny, Nat. Phys., 2015, 11, 427–434.

26 P. Y. Lin, T. Wu, M. Ahmadi, L. Liu, S. Haacke, T. F. Guo and B. Hu, Nano Energy, 2017, 36, 95–101.

27 M. A. Cabero Zabalaga, J. Wei, H. Yang, B. B. Fan, Y. Sun and W. Zhao, ACS Omega, 2017, 2, 7777–7783.

28 M. Klein, R. Pankiewicz, M. Zalas and W. Stampor, Sci. Rep., 2016, 6, 30077.

29 T. Geiger, S. Kuster, J. H. Yum, S. J. Moon, M. K. Nazeeruddin, M. Gra¨tzel and F. Nu¨esch, Adv. Funct. Mater., 2009, 19, 2720–2727.

30 D. Veldman, I. Pek, S. C. J. Meskers, J. Rgen Sweelssen, M. M. Koetse, S. C. Veenstra, J. M. Kroon, S. S. Van Bavel, J. Loos and R. A. J. Janssen, J. Am. Chem. Soc., 2008, 130, 7721–7735.

31 B. Fan, Y. Maniglio, M. Simeunovic, S. Kuster, T. Geiger, R. Hany and F. Nu¨esch, Int. J. Photoenergy, 2009, 581068.

32 D. Pelczarski, P. Grygiel, K. Falkowski, M. Klein and W. Stampor, Org. Electron., 2015, 25, 362–376. 33 H. Hayashi, Introduction to Dynamic Spin Chemistry, World Scientific, 2004.

34 R. P. Groff, A. Suna, P. Avakian and R. E. Merrifield, Phys. Rev. B: Condens. Matter Mater. Phys., 1974, 9, 2655–2660.

35 E. Frankevich, A. Zakhidov, K. Yoshino, Y. Maruyama and K. Yakushi, Phys. Rev. B: Condens. Matter Mater. Phys., 1996, 53, 4498–4508.

36 J. Kalinowski, J. Szmytkowski and W. Stampor, Chem. Phys. Lett., 2003, 378, 380–387.

37 M. Cox, P. Janssen, F. Zhu and B. Koopmans, Phys. Rev. B: Condens. Matter Mater. Phys., 2013, 88, 1–7.

38 A. Kadashchuk, V. I. Arkhipov, C. H. Kim, J. Shinar, D. W. Lee, Y. R. Hong, J. Il Jin, P. Heremans and H. Ba¨ssler, Phys. Rev. B: Condens. Matter Mater. Phys., 2007, 76, 235205.

39 B. Hu, L. Yan and M. Shao, Adv. Mater., 2009, 21, 1500–1516.

40 A. J. Schellekens, W. Wagemans, S. P. Kersten, P. A. Bobbert and B. Koopmans, Phys. Rev. B: Condens. Matter Mater. Phys., 2011, 84, 75204.

41 T. D. Nguyen, B. R. Gautam, E. Ehrenfreund and Z. V. Vardeny, Phys. Rev. Lett., 2010, 105, 166804.

42 P. Shakya, P. Desai, T. Kreouzis, W. P. Gillin, S. M. Tuladhar, A. M. Ballantyne and J. Nelson, J. Phys.: Condens. Matter, 2008, 20, 452203.

43 Y. Lei, Q. Song, Y. Zhang, P. Chen, R. Liu, Q. Zhang and Z. Xiong, Org. Electron., 2009, 10, 1288–1292.

44 P. A. Bobbert, T. D. Nguyen, F. W. A. Van Oost, B. Koopmans and M. Wohlgenannt, Phys. Rev. Lett., 2007, 99, 216801.

45 V. I. Krinichnyi, E. I. Yudanova and N. G. Spitsina, J. Phys. Chem. C, 2010, 114, 16756–16766.

46 B. Khachatryan, A. H. Devir-Wolfman, L. Tzabari, N. Tessler, Z. V. Vardeny and E. Ehrenfreund, Phys. Rev. Appl., 2016, 5, 44001.

47 B. Khachatryan, A. H. Devir-Wolfman, L. Tzabary, A. Keren, N. Tessler, Z. V. Vardeny and E. Ehrenfreund, Synth. Met., 2015, 60, 8–11.

48 F. Alvarez, A. Alegria and J. Colmenero, Phys. Rev. B: Condens. Matter Mater. Phys., 1991, 44, 7306–7312.

49 J. Wang, A. Chepelianskii, F. Gao and N. C. Greenham, Nat. Commun., 2012, 3, 1191.

50 M. Wohlgenannt and Z. V. Vardeny, J. Phys.: Condens. Matter, 2003, 15, R83–R107.

51 Y. Sheng, T. D. Nguyen, G. Veeraraghavan, O¨. Mermer, M. Wohlgenannt, S. Qiu and U. Scherf, Phys. Rev. B: Condens. Matter Mater. Phys., 2006, 74, 045213.

52 M. K. Etherington, J. Wang, P. C. Y. Chow and N. C. Greenham, Appl. Phys. Lett., 2014, 104, 063304.